CIRP Annals - Manufacturing Technology 58 (2009) 77–80

Contents lists available at ScienceDirect

CIRP Annals - Manufacturing Technology

journal homepage: http://ees.elsevier.com/cirp/default.asp

A finite element modeling approach to predicting white layer formation in nickel superalloys

S. Ranganath [a], C. Guo (2)[a,*], P. Hegde [b]

[a] United Technologies Research Center, 411 Silver lane, East Hartford, CT 06 108, USA
[b] Kennametal Inc., Latrobe, PA, USA

ARTICLE INFO

Keywords:
Machining
Nickel alloy
White layer

ABSTRACT

This paper presents a finite element (FE)-based model to predict critical parameters for the formation of white layer and bent grains in finish-machining of a nickel superalloy. A "piece-wise" Johnson–Cook model was constructed for describing the material flow behavior. Chips predicted and collected during orthogonal turning tests show clear shear banding even under low-speed. The machined surfaces contain a distorted layer with elongated grains. The ratio of edge radius to uncut chip thickness is found to be the most dominant factor in determining the amount of plastic strain in the machined surfaces, which is believed to be the cause for white layer and bent grains in low-speed machining of nickel alloys.

1. Introduction

The superior hot-hardness of nickel super alloy makes it the most difficult to machine material [1]. Subsurface damages such as white layer and bent grains often appear even under low-speed machining. It is called white layer because it appears featureless or white under a light microscope. The subsurface may also contain a severely deformed layer from a few to several microns in thickness where the gamma prime or grains are bent and elongated. The distorted grains in this zone have aspect ratios of more than 2–6 times as compared to the original equiaxed grain structure (Fig. 1). The white layer and bent grains have shown to be detrimental to the Low Cycle Fatigue (LCF) life of the machined components under high stress and high temperature applications.

White layers were also found on metal surfaces produced by various manufacturing processes such as machining, EDM, grinding and forming [2]. It also appeared on surfaces of service parts such as locomotive rails, gear surfaces, and pin-on-disk wear test surfaces [1–4]. White layer formation in machining of different materials such as hardened steels and brass have been evaluated in the past [5–12], though very few investigations have focused on nickel superalloys [5,12,13]. White layer is known to occur both with phase transformation, as well as under conditions where temperature rise is too low for phase transformations [11]. Griffiths [2] proposed three possible mechanisms: phase transformation due to rapid heating and quenching, fine grain structure formed due to severe plastic deformation, and reaction of the surface with the environment.

Extensive machining trials together with metallurgical evaluations of the machined surfaces are required to develop machining processes for aerospace components. Cut-ups of machined components are often required as a means for quality insurance. The goal of the present research is to develop predictive machining models to investigate the root causes of machining-induced white layer formation and to select machining parameters to achieve white layer free superalloy finish machining.

In this paper, a finite element analysis (FEA) model is developed and a "piece-wise" Johnson–Cook model was constructed to describe the flow stress behavior of nickel alloys. A set of controlled orthogonal machining tests were performed to collect data to validate the model. The established model was used to predict plastic strain on the machined surfaces under various conditions. The results show that the ratio of edge radius to uncut chip thickness is the most important parameter in controlling the plastic strain and temperature on the machined surface.

2. Experimental investigations

Orthogonal turning tests were performed on the end faces of cylindrical bars of diameter 64 mm and thickness 34 mm as shown in Fig. 2. The workpiece material is a commercial IN100 nickel superalloy. Grooves were made on the end faces of the bars to create circular rings for orthogonal machining. The test matrix is given in Table 1. No coolant was employed and a new tool edge was used for each test. Profilometry methods were used to measure the insert edge hones and curve fitting techniques were used to establish the edge parameters. The measured edge radii are 10 and 25 μm for the carbide and CBN inserts, respectively.

The collected chips were mounted, polished, etched (lactic/nitric-base solution), and observed under optical and/or scanning electron microscopes. Examples of the chips collected are shown in Fig. 3. The chips show clear segmentations with distinct shear bands under all cutting conditions. A simple method was employed to measure chip thickness where the maximum and minimum values were averaged. The chip ratio and strain were calculated using the Merchant model. Chip segmentation spacings

---

* Corresponding author.

0007-8506/$ – see front matter © 2009 CIRP.
doi:10.1016/j.cirp.2009.03.109

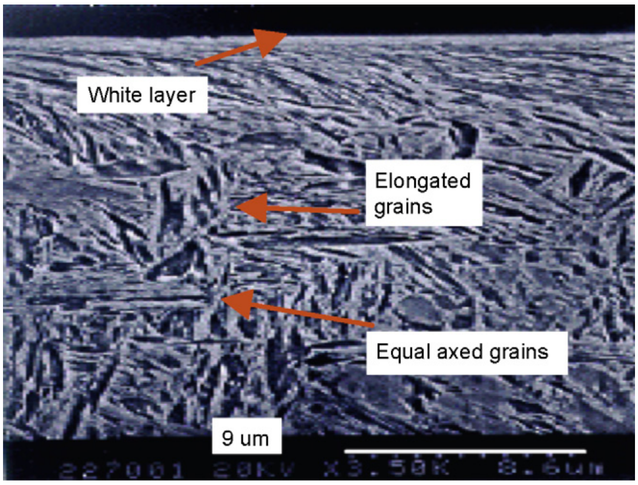

Fig. 1. White layer and deformed layer [20].

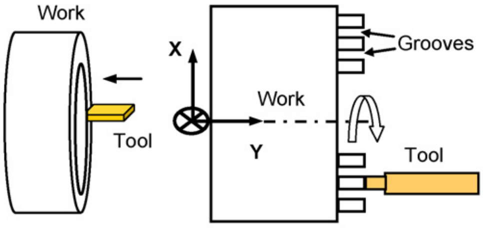

Fig. 2. Orthogonal cutting test schematic.

Table 1
Parameters for machining tests.

Test	h_c (µm)	Cutting speed (m/min)	Inserts
1	30	4	Carbide, KC5510, CNGG432FS, $r_\beta = 10$ µm, $\gamma_e = -6°$
2	60	4	
3	30	40	
4	60	40	
5	30	40	CBN, CNGA432EMT, $r_\beta = 25$ µm, $\gamma_e = -6°$
6	60	40	
7	30	120	
8	60	120	

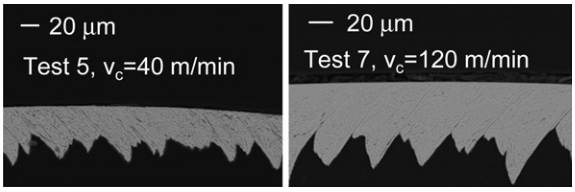

Fig. 3. Chips with carbide tool.

Table 2
Measured chip morphology parameters.

Test	Average h_c (µm)	Chip ratio	Chip strain	Segmentation spacing (µm)
1	115	0.26	3.8	38
2	87	0.69	1.4	36
3	90	0.33	2.9	30
4	107	0.56	1.7	27
5	53	0.57	1.9	35
6	72	0.83	1.3	46
7	65	0.46	2.3	46
8	No measurements			41

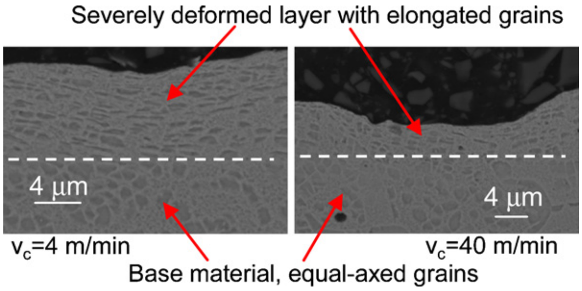

Fig. 4. SEM micrograph of sample.

were also measured under microscope and all results are summarized in Table 2.

The machined specimens were sectioned, mounted, polished, etched and observed under SEM. Severe subsurface deformation was observed in all cases as shown in Fig. 4. The grains near the machined surfaces are elongated by the machining action. The machined surfaces show no white layer because a new cutting edge was used for each test and the cutting time was short.

Nano-hardness measurements were also performed on the machined cross-sections. The deformed layers appear ~2–3 times harder than the base material with the hardness being higher under low speed cases with blunt edged tools (large edge radius, negative effective rake angle). The increased hardness of the distorted layer near the machined surface indicates the dominance of strain hardening.

3. Material properties for FEA modeling

Accurate modeling of the material behavior is the key for FE-based machining modeling. The material behavior will determine how damage occurs and progresses when material is deformed. The triggering of adiabatic shearing is also mainly determined by the material behavior.

High strain rate compression tests and machining tests have been used to obtain flow stress data. Several phenomenological plasticity models such as power law, Johnson–Cook [14], Maekawa [15], and Zerilli [16] have been developed to relate flow stress to plastic strain, strain rate and temperature. Superalloys are designed to have an almost uniform flow stress until certain high temperatures. The resulting flow–stress behavior cannot be adequately captured with a simple JC model as shown in Fig. 5 for an Inco 718.

In this paper, a "piece-wise" Johnson–Cook model was proposed to represent the plasticity behavior of IN100. This model employs two separate Johnson–Cook equations. In the low temperature range (below 800 °C), the stress variations are primarily fixed by the microstructural components, or the distribution of the primary and secondary γ' phase. This gives an almost uniform flow stress, with minimal dependency on

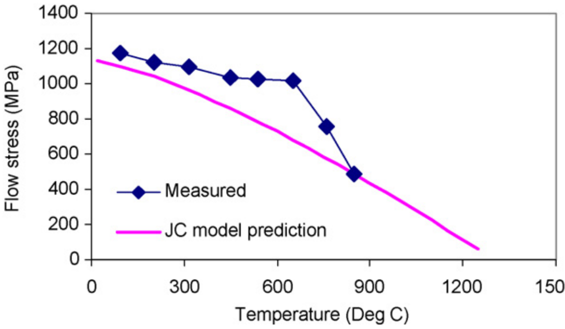

Fig. 5. Inco 718 flow stress JC model prediction.

Table 3
Piece-wise Johnson–Cook models (IN100).

A	B	n	m	c	$\dot{\varepsilon}_0$	T (°C)
1150	3410	0.98	4.47	0.0132	0.001	20–870
1150	3410	0.98	0.56	0.0532	0.001	870–1220